Monthly Notices
of the
ROYAL ASTRONOMICAL SOCIETY

MNRAS **458,** 613–623 (2016) doi:10.1093/mnras/stw312
Advance Access publication 2016 February 11

Hunting down systematics in baryon acoustic oscillations after cosmic high noon

Francisco Prada,[1,2,3]★ Claudia G. Scóccola,[1,4,5,6,7,8]★ Chia-Hsun Chuang,[1]† Gustavo Yepes,[4] Anatoly A. Klypin,[9] Francisco-Shu Kitaura,[10] Stefan Gottlöber[10] and Cheng Zhao[11]

[1]*Instituto de Física Teórica, (UAM/CSIC), Universidad Autónoma de Madrid, Cantoblanco, E-28049 Madrid, Spain*
[2]*Campus of International Excellence UAM+CSIC, Cantoblanco, E-28049 Madrid, Spain*
[3]*Instituto de Astrofísica de Andalucía (CSIC), Glorieta de la Astronomía, E-18080 Granada, Spain*
[4]*Departamento de Física Teórica, Universidad Autónoma de Madrid, Cantoblanco, E-28049 Madrid, Spain*
[5]*Instituto de Astrofísica de Canarias (IAC), C/Vía Láctea, s/n, La Laguna, E-38205 Tenerife, Spain*
[6]*Dpto. Astrofísica, Universidad de La Laguna (ULL), E-38206 La Laguna, Tenerife, Spain*
[7]*Facultad de Ciencias Astronómicas y Geofísicas - Universidad Nacional de La Plata. Paseo del Bosque S/N (1900), La Plata, Argentina*
[8]*CONICET, Rivadavia 1917, 1033Buenos Aires, Argentina*
[9]*Astronomy Department, New Mexico State University, Las Cruces, NM 88003, USA*
[10]*Leibniz-Institut fuer Astrophysik (AIP), An der Sternwarte 16, D-14482 Potsdam, Germany*
[11]*Tsinghua Center for Astrophysics, Department of Physics, Tsinghua University, Haidian District, Beijing 100084, P. R. China*

Accepted 2016 February 8. Received 2015 December 27; in original form 2014 November 14

ABSTRACT

Future dark energy experiments will require accurate theoretical predictions for the baryon acoustic oscillations (BAOs). Here, we use large *N*-body simulations to study any systematic shifts and damping in BAO due to non-linear effects. The impact of cosmic variance is largely reduced by dividing the tracer power spectrum by that from a 'BAO-free' simulation starting with the same random amplitudes and phases. The accuracy of our simulations allows us to resolve well dark matter (sub)haloes, which permits us to study with high accuracy (better than 0.02 per cent for dark matter and 0.07 per cent for low-bias haloes) small BAO shifts α towards larger k, and non-linear damping $\Sigma_{\rm nl}$ of BAO in the power spectrum. For dark matter, we provide an accurate parametrization of the evolution of α as a function of the linear growth factor $D(z)$. For halo samples, with bias from 1.2 to 2.8, we measure a typical BAO shift of $\approx$0.25 per cent, with no appreciable evolution with redshift. Moreover, we report a constant shift as a function of halo bias. We find a different evolution of the BAO damping in all halo samples as compared to dark matter with haloes suffering less damping, and also find some weak dependence on bias. Larger BAO shift and damping are measured in redshift-space, which can be explained by linear theory due to redshift-space distortions. A clear modulation in phase with the acoustic scale is observed in the scale-dependent halo bias due to the presence of BAOs. We compare our results with previous works.

Key words: galaxies: haloes – galaxies: statistics – dark matter – large-scale structure of Universe.

1 INTRODUCTION

The discovery of cosmic acceleration has motivated the development of large experiments that aim at measuring the expansion history of the Universe and growth of structure with high precision at the 0.1–1 per cent level. More precise measurements of the baryon acoustic oscillation (BAO) scale rely on ongoing and future large galaxy, quasars and Ly α surveys and improved analysis techniques. This field has undergone an enormous progress since the BAO peak was detected for the first time in the SDSS-II and 2dFGRS galaxy clustering statistics (Cole et al. 2005; Eisenstein et al. 2005). The SDSS-III/BOSS survey, with almost 4 yr of data, has already reached 1.0 per cent precision on measuring the baryon acoustic scale using the DR11 CMASS sample of massive galaxies at $z = 0.57$ (Anderson et al. 2014). This is a significant achievement compared to the 4 per cent precision of the first SDSS-II LRG

★ E-mail: fprada@iaa.es (FP); cscoccola@fcaglp.unlp.edu.ar (CGS)
† MultiDark Fellow.

measurements. It is worth mentioning the BAO measurements that have been conducted at $z \sim 0.35$ using the SDSS-II DR7 LRG (e.g. Percival et al. 2007; Sanchez et al. 2009; Reid et al. 2010; Chuang, Wang & Hemantha 2012; Padmanabhan et al. 2012) and WiggleZ (Blake et al. 2011) $z \sim 0.6$ survey data.

With the completion of BOSS after DR12, the 1 per cent precision will be superseded by new experiments such as DESI (Schlegel et al. 2011; Levi et al. 2013) and *Euclid* (e.g. Laureijs et al. 2011). Both surveys aim at measuring the BAO scale to the subpercent level over a wide redshift range $0.5 < z < 3.5$, thus, providing unprecedented constraints on the dark energy equation of state (see Weinberg et al. 2013 for a complete review and forecasts on cosmological models with current and future planned BAO experiments). The new generation dark energy experiments also impose severe challenges on understanding any possible systematic shifts in the BAO signature due to non-linear gravitational growth, scale-dependent bias and redshift-space distortions (RSD) to a high precision, better than the measured statistical uncertainties. This challenge has motivated in the recent years many works based on perturbation theory and large-volume *N*-body simulations to understand the damping and shifts of the BAO feature as being probed by dark matter and biased tracers (e.g. Angulo et al. 2008; Crocce & Scoccimarro 2008; Sánchez, Baugh & Angulo 2008; Seo et al. 2008; Smith, Scoccimarro & Sheth 2008; Padmanabhan & White 2009; Seo et al. 2010; Mehta et al. 2011; Sherwin & Zaldarriaga 2012; Wang & Zhan 2013; Angulo et al. 2014; Rasera et al. 2014).

A shift in the acoustic scale of $\alpha - 1 \sim 0.3$ [per cent] has been measured in the dark matter power spectrum at $z = 0$ using *N*-body simulations, where α is the ratio of the linear BAO scale to the measured scale. In this case, the BAO feature is found towards larger k, relative to the linear $P(k)$ (see e.g. Seo et al. 2010). This shift, and its dependence with redshift, has been well explained by perturbation theory in numerous works as due to additional oscillations generated by non-linear mode coupling effects (e.g. Crocce & Scoccimarro 2008; Padmanabhan & White 2009; Sherwin & Zaldarriaga 2012). From the results of a couple of simulations, each of volume $(2\,h^{-1}\,\mathrm{Gpc})^3$ and 576^3 particles (with force resolution $173.6\,h^{-1}$kpc), Seo et al. (2010) measured the mean BAO shift at $z = 0.3$, 1.0 and 3.0 and found an evolution of the shift as $\alpha(z) - 1[\mathrm{per\,cent}] = (0.295 \pm 0.075)[D(z)/D(0)]^{1.74 \pm 0.35}$. The measured power index is close to the expected $D(z)^2$ prediction from perturbation theory (see Padmanabhan & White 2009; Sherwin & Zaldarriaga 2012). Regarding the shift in dark matter haloes, most of the simulation data used for these measurements considered only distinct haloes based on Friend-of-Friend (FoF) halo finders, and often they incorporate substructures (subhaloes) by adopting a halo occupation distribution (HOD) model (see e.g. Padmanabhan & White 2009; Mehta et al. 2011). For example, Mehta et al. (2011), using the same simulations than Seo et al. (2010), did not detect any shift in the acoustic scale for their HOD models with $b < 3$ biased tracers; typically they measured a shift of 0.1 per cent $\pm$ 0.1 per cent. However, their most biased HOD models showed a shift of moderate significance (0.75 $\pm$ 0.31 per cent). Few years earlier, Sánchez et al. (2008) found negative shifts of 0.3–0.6 per cent at $z = 0$ for halo samples with bias 2–2.5, based on FoF haloes drawn from an ensemble of moderate resolution simulations. More recent analysis based on applying semi-analytical models of galaxy formation to the Millennium-XXL simulation reported, at redshift $z = 1$, BAO shifts with respect to the dark matter case smaller than $\pm$0.2 per cent and smaller than 0.5 per cent for their densest and lowest density galaxy samples, respectively (see Angulo et al. 2014). Wang & Zhan (2013) suggested that the non-linear damping of the BAO signal is less severe for haloes than for dark matter (see also Angulo et al. 2014).

On the other hand, perturbation theory does not provide a solid prediction for these shifts in the halo clustering statistics. The shift seems to depend on two halo bias parameters, b_1 and b_2, which in principle will cause possible arbitrary shifts of the acoustic scale (see Padmanabhan & White 2009).

In this work, we investigate and measure the evolution of the non-linear shift of the acoustic scale in the dark matter halo power spectrum relative to the underlying dark matter distribution taking advantage of the new suite of BigMultiDark (hereafter BigMD) simulations, which combines high resolution with large volume for the adopted Λ cold dark matter (ΛCDM) Planck cosmological model. The BigMD simulations are designed to have sufficient resolution to resolve haloes and subhaloes within a cubic box of $2.5\,h^{-1}$ Gpc on a side with a completeness suitable to study the clustering of galaxies hosted by halo samples with bias down to 1.2 at $z = 0$. This permits us to study with high accuracy (better than 0.02 per cent for dark matter and 0.07 per cent for low-bias haloes) small BAO shifts α towards larger k, and non-linear damping $\Sigma_{\rm nl}$ of BAO wiggles in the power spectrum from redshift 1 to the present. The effect of cosmic variance is largely reduced by dividing the tracer power spectrum by that from a BAO-free simulation starting with the same phases. For consistency, we have also measured the damping of acoustic oscillations both for dark matter and halo biased tracers. These new results clarify the previously reported measurements found in the literature.

The paper is organized as follows. In Section 2, we introduce the BigMD simulation data used in our study. In Section 3, we describe the details of the methodology adopted to measure the BAO shift and damping for dark matter and various halo samples. In Section 4, we present our main results, and we summarize and conclude in Section 5.

2 SIMULATIONS FOR LARGE GALAXY SURVEYS

Fig. 1 displays an overview of the basic numerical (force and mass resolution) and cosmological parameters adopted in state-of-the-art cosmological simulations, comprising at least one $(h^{-1}\,\mathrm{Gpc})^3$ in volume, carried out to study galaxy clustering and bias for large galaxy surveys (i. e. Horizon, MICE7680/MICE3072, LD-Carmen/LD-Oriana, Horizon2/Horizon3, DEUS-FUR, MXXL, MDR1, zHorizon, BigMD-suite/MDPL, Coyote, Jubilee, and DarkSky by Teyssier et al. 2009; Crocce et al. 2010; Lawrence et al. 2010; McBride et al. 2009; Kim et al. 2011; Alimi et al. 2012; Angulo et al. 2012; Prada et al. 2012; Watson et al. 2013; Klypin et al. 2014; Skillman et al. 2014; Smith et al. 2014; respectively). In the left-hand panel, for each simulation box we plot the number of particles per unit comoving distance (and the mass resolution for haloes with at least 100 particles) versus the simulation box length. The size of the circles are inversely proportional to the softening parameters, ϵ, used in the gravitational force: the larger circle corresponds to MultiDark Planck (MDPL) with $\epsilon = 5\,h^{-1}$ kpc and the smallest to the Horizon-3 run with $\epsilon = 150\,h^{-1}$ kpc. We show, in the right-hand panel, some of the cosmological parameters assumed in each simulation, $n_{\rm s}$ (the spectral index of the primordial power spectrum) and σ_8 (the root mean square – rms – amplitude of linear mass fluctuations in spheres of $8\,h^{-1}$ Mpc comoving radius at redshift $z = 0$), compared with the Planck 68 and 95 per cent confidence level contours assuming a flat ΛCDM cosmology (Planck Collaboration XVI 2014).

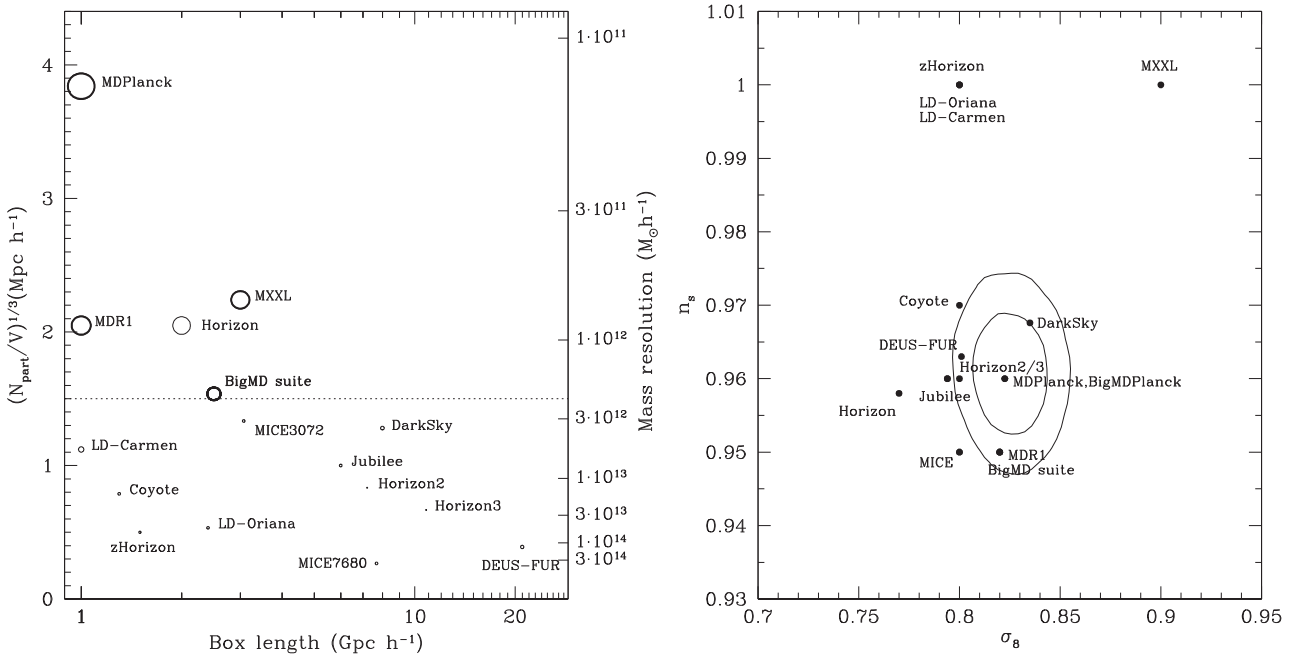

Figure 1. Left: compilation of the basic numerical parameters adopted in large N-body cosmological simulations used in recent years for galaxy clustering and bias studies. The number of particles per unit comoving distance (and mass resolution for haloes with at least 100 particles) is shown as a function of the box length for each simulation. The size of the circles is inversely proportional to the softening parameter ϵ used in the gravitational force. Our new suite of BigMD simulations have been designed to meet all science requirements needed to interpret the galaxy clustering in the BOSS survey (dotted line). Right: n_s versus σ_8 (right) cosmological parameters adopted for each simulation. Contours show 68 and 95 per cent confidence levels from Planck assuming a flat ΛCDM Planck cosmology. In this work, we are using the BigMD Planck simulations.

The BigMD-suite of ΛCDM simulations have been designed to meet the science requirements of the BOSS galaxy survey, i.e. the numerical requirements for mass and force resolution that allows us to resolve well those haloes and subhaloes that can host typical BOSS massive galaxies at $z \sim 0.5$, which will permit to create mock catalogues with the appropriate galaxy bias and clustering. The baseline of the BigMD N-body simulations comprises 3840^3 particles in a box with $2.5\,h^{-1}$ Gpc on a side. Initial conditions were set at the redshift $z_{\rm init} = 100$ with identical Gaussian fluctuations for all simulations. We used GINNUNGAGAP,[1] a publicly available full MPI+OpenMP initial conditions generator code that uses Zeldovich approximation (ZA) with an unlimited number of particles. Because our simulations start at high redshift $z_{\rm init} = 100$, the effects of using ZA instead of more accurate second-order perturbation theory (2lpt) is rather small. For example, Schneider et al. (2015) find that the non-linear dark matter power spectrum is ∼0.5 per cent lower for ZA initial conditions for BAO scales $k = 0.1$–$0.5\,h\,{\rm Mpc}^{-1}$. We made our own test with ZA and 2lpt initial conditions by running two simulations with 1024^3 particles in a 1 Gpc h^{-1} simulation box. We find similar results for the dark matter power spectrum: $P_{\rm ZA}/P_{\rm 2lpt} - 1 \approx 5 \times 10^{-3}$ for $k = 0.05$–$0.5\,h\,{\rm Mpc}^{-1}$. We also identified haloes and subhaloes. For the number density similar to the BOSS CMASS sample, the errors on halo power spectrum have similar magnitude of ∼0.5 per cent. Note that these errors are the rms deviations of point-by-point estimates of $P_{\rm ZA}/P_{\rm 2lpt}$. Errors in the BAO fits (offset and shift) are significantly smaller.

The BigMD simulations were run with the L-GADGET-2 code (see Klypin et al. 2014, for details). In this work, we use a couple of those simulations where we adopted the cosmological parameters based on the fits to the Planck data (Planck Collaboration XVI 2014). The mass and force resolutions are $2.36 \times 10^{10}\,h^{-1}\,{\rm M}_\odot$ and $10\,h^{-1}$ kpc. The choice of numerical parameters to meet our requirements (combination of mass and force resolutions is highlighted with a dashed-line in Fig. 1) were chosen after the completion of many tests to study the convergence for the correlation function and circular velocities for haloes and their subhaloes (see Klypin et al. 2015, for details). This allows us to resolve well the internal structure of (sub)haloes, thus, making possible to connect them with BOSS-like galaxies.

Dark matter haloes (and subhaloes) were identified with a parallel version of the Bound-Density-Maxima (BDM) algorithm (Klypin & Holtzman 1997; Riebe et al. 2013). BDM is a spherical overdensity code that provides many properties of haloes and subhaloes in our BigMD simulations. We then use a simple, non-parametric halo abundance matching (HAM) prescription, to connect dark matter (sub)haloes with galaxies by selecting them above a given maximum circular velocity $V_{\rm max}$. This procedure is able to predict the clustering properties, and the HOD of observed galaxies for different number densities (e.g. Conroy, Wechsler & Kravtsov 2006; Trujillo-Gomez et al. 2011; Nuza et al. 2013). We selected four different halo samples from the BigMD BDM catalogues for our analysis with number densities $2 \times 10^{-3}, 1 \times 10^{-3}, 4 \times 10^{-4}, 2 \times 10^{-4}\,{\rm h}^3\,{\rm Mpc}^{-3}$, corresponding to linear biases 1.56, 1.76, 2.04, and 2.28 at several redshifts up to $z = 1$ (see Fig. 2), of typical Emission Line Galaxies (ELGs) and Luminous Red Galaxies (LRGs) as those being targeted in the major surveys discussed here. It should be noted that the limitations of using $V_{\rm max}$ instead of the maximum value of $V_{\rm max}$ over history when connecting haloes to galaxies, which provides better performance on describing the clustering of LRGs (see Nuza et al.

[1] http://code.google.com/p/ginnungagap

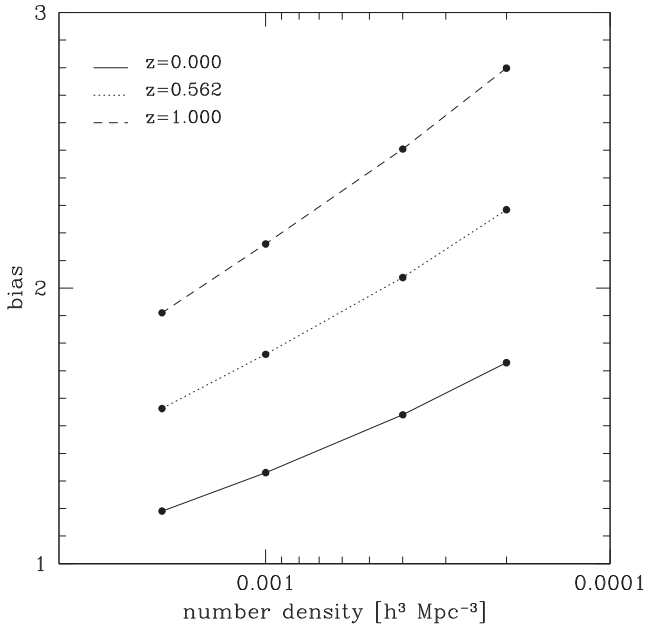

Figure 2. Bias as a function of number density at $z = 0$, 0.562, and 1, for four different samples of dark matter haloes selected accordingly to their maximum circular velocities $V_{\rm max}$ from our BigMD Planck simulations.

2013). In the case of ELGs, the new clustering data from the SDSS-III/eBOSS survey will reveal us the limitations of using HAM for modelling their clustering signal.

3 MEASURING THE SHIFT AND DAMPING OF THE ACOUSTIC SCALE

The analysis performed in this work on the non-linear evolution of the shift and damping of acoustic oscillations in the power spectrum of dark matter and the halo samples mentioned above, is based on two simulations of our BigMD suite. The first one, BigMDPL, adopted the initial matter power spectrum generated using CAMB (Lewis, Challinor & Lasenby 2000) with the Planck cosmological parameters; and for the second BigMDPLnw simulation, the same cosmological parameters were assumed but with a smooth initial power spectrum with no BAO wiggles, generated by fitting a cubic spline (Press et al. 1992) to the CAMB table with three nodes fixed empirically. We recall that the initial conditions of both simulations were generated with the same random amplitudes and phases. Hence, the effect of cosmic variance is greatly reduced when dividing the spectrum $P(k)$ computed from BigMDPL with BAOs, for a given tracer, by the non-wiggle BigMDPLnw power spectrum $P_{\rm nw}(k)$. This allows us to obtain measurements with high accuracy of the BAO stretch parameter α and damping as a function of redshift. Below, we provide more details on the uncertainty in the BAO shift measurements.

We compute P(k) using 285 linear bins, in the k-range (0.085,0.8). The limits are chosen to contain the BAO oscillations, and have large enough range at smaller scales where BAO have effectively vanished out, which allows us to estimate the errors. We compute the error for each redshift (and each number density, in the case of haloes) separately. To do so, we take the statistical error of the measurement as the scatter of the ratio $P(k)/P_{\rm nw}(k)$ at large values of k, where the BAO have effectively vanished. We use a Fourier mesh of 2500^3 cells in a box size of $(2.5\ h^{-1}\ {\rm Gpc})^3$. Density fields are calculated using the cloud-in-cell assignment scheme, and aliasing and shot noise corrections were applied. To improve the convergence of the fitting, in redshift-space, and only for the haloes, we reduced the k-range to (0.085,0.6), and therefore the number of linear bins used was 205.

Fig. 3 shows the spherically average power spectra at $z = 0$ in real-space drawn from BigMDPL, divided by the corresponding non-wiggle BigMDPLnw power spectrum for dark matter (top-left panel) and a typical halo sample with number density $1 \times 10^{-3}{\rm Mpc}^{-3}h^3$ and $bias = 1.33$ (top-right panel). We measure the shift of the BAO relative to linear theory by following a similar methodology as that presented in Seo et al. (2008). For a given tracer, the power spectrum with wiggles is modelled by damping the acoustic oscillation features of the linear power spectrum assuming a Gaussian with a scale parameter $\Sigma_{\rm nl}$ which accounts for the BAO broadening due to non-linear effects (e.g. Eisenstein, Seo & White 2007), i.e.

$$P(k) = \Big[\left(P^{\rm lin}(k) - A(k)P^{\rm lin}_{\rm nw}(k)\right) \exp\left(-k^2\Sigma^2_{\rm nl}/2\right) + A(k)P^{\rm lin}_{\rm nw}(k) \Big] B(k), \quad (1)$$

where $P^{\rm lin}$ is the linear power spectrum generated with CAMB, adopting the Planck cosmology, and $P^{\rm lin}_{\rm nw}$ is the smooth non-wiggle spline power spectrum. $B(k)$ represents the non-linear growth of the matter power spectrum, which in the case of haloes includes also a scale-dependent bias. The $A(k)$ term allows for any correction that might be needed to account for the proper description of the broad-band shape of the power spectrum. Note that $A(k) = 1$ for an ideal case.

We then fit the ratio $P/P_{\rm nw}$ of the power spectrum with acoustic oscillations to that with no-BAO drawn from the BigMDPL/BigMDPLnw simulation pair (see Fig. 3) with the following formula,

$$P(k)/P_{\rm nw}(k) = \left[\left(\frac{P^{\rm lin}(k/\alpha)}{A(k)P^{\rm lin}_{\rm nw}(k/\alpha)} - 1 \right) \exp\left(-k^2\Sigma^2_{\rm nl}/2\right) + 1 \right] C(k), \quad (2)$$

where $C(k)$ accounts for the non-linear growth of both wiggle $P(k)$ and non-wiggle $P_{\rm nw}(k)$ power spectra. Similar to Anderson et al. (2014), we adopt simple power-law polynomials for both $A(k)$ and $C(k)$ terms expressed in the form $a_0k^{a_1}$ and $c_0k^{c_1}$, respectively. The shift and damping of the acoustic oscillations, measured by α and $\Sigma_{\rm nl}$, are considered free parameters in our fit. For the χ^2 analysis, we have six fitting parameters $\{\alpha,\ \Sigma_{\rm nl},\ a_0,\ a_1,\ c_0,\ c_1\}$, and the fit is performed over the wavenumber range $0.085 < k < 0.8\ h\ {\rm Mpc}^{-1}$ (vertical dotted lines in Fig. 3). The errors on the parameters are computed after marginalizing over all the other parameters. We assume a diagonal covariance matrix, which was tested to be a good approximation. Note that we avoid in the fit the first acoustic peak being distorted, up to some extent, by our own choice of the broad-band shape of the power spectrum when we build the featureless ('BAO free') power spectrum $P_{\rm nw}(k)$. The χ^2 per degree of freedom $\chi^2/d.o.f.$, which indicates the goodness-of-fit between our model and the BigMD simulation data, is 1.011 and 0.911 for the ratio of the wiggle to non-wiggle power spectra for dark matter and the halo sample shown in Fig. 3. The solid line corresponds to the best-fitted model given by equation (2). The damping of the BAO features is clearly seen in both dark matter and haloes when compared with the linear wiggle to non-wiggle $P(k)$ ratio (thin solid line).

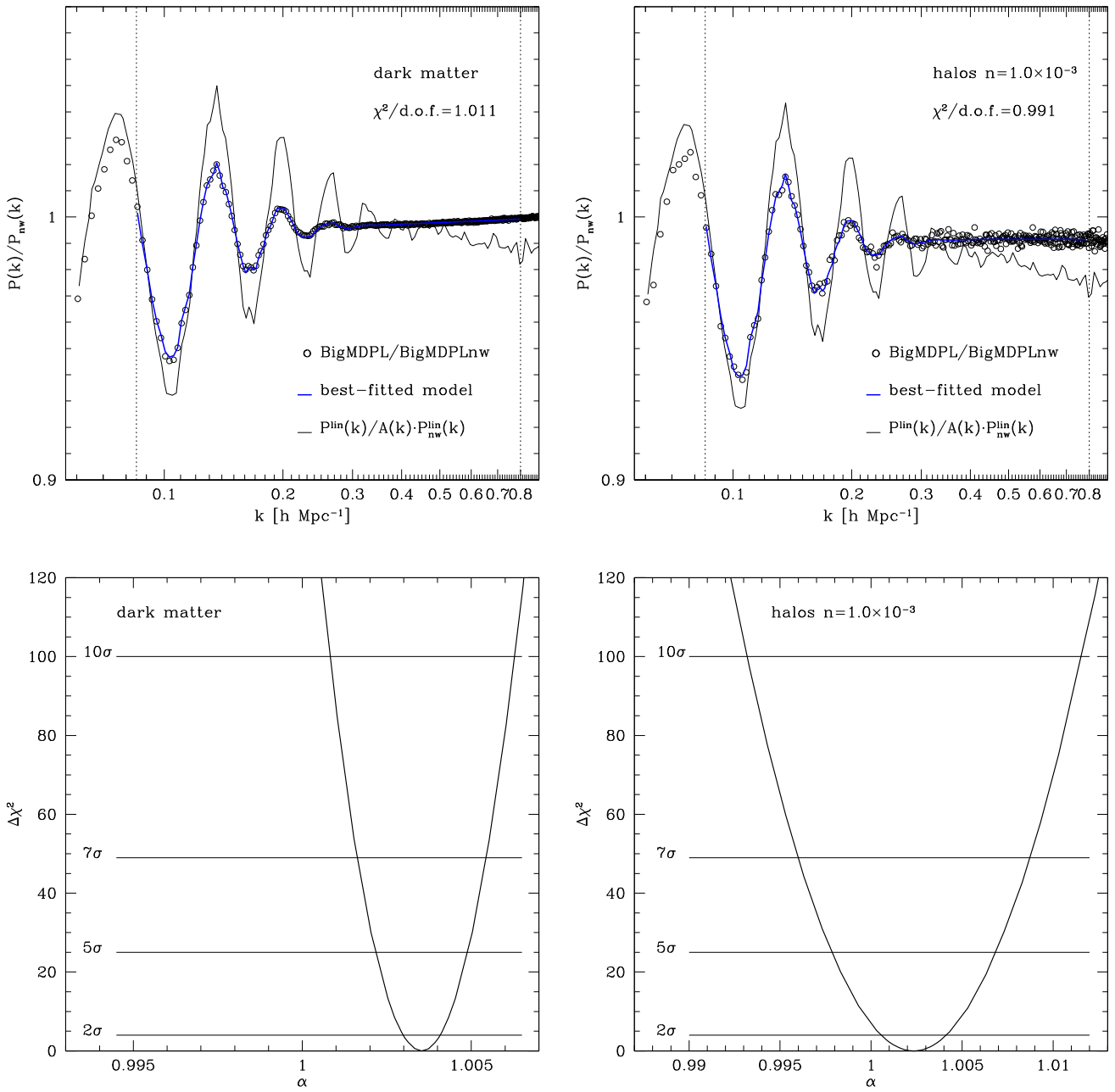

Figure 3. Power spectra at $z = 0$, in real-space, divided by the corresponding non-wiggle power spectrum obtained from BigMDPL and BigMDPLnw, respectively, for dark matter (top-left panel) and a typical halo sample with number density 1×10^{-3} Mpc^{-3} h^3 (top-right panel). The thick solid line corresponds to the best-fitted model given by equation (2) in the wavenumber range $0.085 < k < 0.8\ h$ Mpc^{-1} shown by the vertical dotted lines. The ratio of wiggle and non-wiggle linear matter power spectrum is also shown in both cases (thin solid line). The bottom panels show the likelihood χ^2 distributions for the BAO shift α parameter both for dark matter (left-hand panel) and the halo sample (right-hand panel).

There are two main contributions to the uncertainty in the BAO shift estimates.

(i) Random errors in estimates of the power spectrum. There is a finite number of independent harmonics contributing to the power in each bin in k-space used to estimate the power spectrum. The amplitude of each harmonic is a random number with Gaussian distribution. The finite number of the harmonics results in a random error in the estimate of $P(k)$.

(ii) Non-linear mode-coupling may result in additional errors. The simulation including BAO wiggles will experience larger gravitational interactions at the scale of the BAO leading to correlated errors in the estimates of $P(k)$.

The propagation of these two kinds of errors in the estimates of the power spectra lead to uncertainties in the ratio $P(k)/P_{\rm nw}(k)$. To acquire some knowledge of the magnitude of such errors in the ratio $P(k)/P_{\rm nw}(k)$, we use the PATCHY code (Kitaura, Yepes & Prada 2014; Kitaura et al. 2015) to generate a large number of non-linear density field realizations. The PATCHY code uses Lagrangian perturbation theory (LPT) and a non-linear, scale-dependent stochastic biasing scheme to produce halo realizations of the density field. In

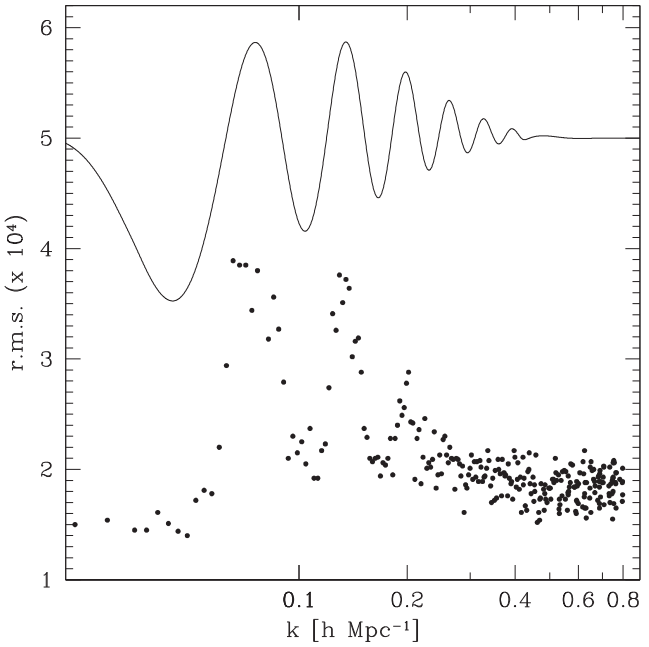

Figure 4. Errors in the power spectrum in real-space due to shot noise and mode coupling (dots). The errors are measured using 100 pairs of PATCHY simulations with and without BAO wiggles, but sharing the same white noise (see the text). The errors are dominated by mode coupling. To indicate the correlation between the maxima of the mode-coupling and the BAO peaks we show the initial $P/P_{\rm nw}$ from CAMB, scaled with an appropriate factor for visualization purposes (thin line).

particular, it uses augmented LPT (ALPT; Kitaura & Heß 2013), to generate a dark matter density field on a mesh starting from Gaussian fluctuations and to compute the peculiar velocity field. ALPT is based on a combination of second-order LPT (2LPT) on large scales and the spherical collapse model on smaller scales. PATCHY also accounts for the missing power of perturbative approaches w.r.t. *N*-body simulations.

For our estimates, we generated 100 pairs of PATCHY matter density fields at $z = 0$ with and without BAO wiggles, but sharing the same white noise. As one can see in Fig. 4 the dispersion peaks, as expected, at the BAO positions (as a reference, we also plot the initial $P/P_{\rm nw}$ ratio from CAMB, scaled with an appropriate factor for visualization purposes, thin line). However, the mode-coupling errors are smaller than the dispersion in the measurement of the $P/P_{\rm nw}$ ratio in our BigMD simulation, shown in Fig. 3, which are of the order of $\sim 5 \times 10^{-4}$. The residual noise at large k's comes from power from smaller k's at the BAO scale as shown in Neyrinck & Yang (2013, see upper panel in their fig. 3).

Therefore, to be conservative, we adopt for the Chi-square fitting the error estimated from the dispersion in the wavenumber range $0.5 < k < 0.8\ h\ {\rm Mpc}^{-1}$ that is free of oscillation features, and as mentioned above, has a level of uncertainty, $\sim 5 \times 10^{-4}$, larger than the effects due to mode-coupling, i.e. $< 4 \times 10^{-4}$. We assume a k-independent value of the rms. For many of the cases (redshifts and number densities), this seems to be the case, even from visual inspection. In other cases, there is a small tilt in the ratio $P/P_{\rm nw}$, even for the model. In these cases, we first fit the tilt, and then consider the dispersion with respect to it. For completeness, we show the error used for each of the fitting cases in Table 1.

As mentioned above, the dilation (shift) parameter α yields the relative position of the acoustic scale in our Planck simulations w.r.t. the model adopted in equation (2). From our fit, we measure for the dark matter tracer at $z = 0$ a small BAO shift $\alpha - 1[\text{per cent}] = 0.353^{+0.027}_{-0.026}$ for the data shown in Fig. 3. This indicates a shift of the acoustic scale towards larger k, relative to the linear power spectrum, which has been measured with high accuracy. For the data of the halo biased tracer sample shown in Fig. 3, we measure a shift $\alpha - 1[\text{per cent}] = 0.236^{+0.086}_{-0.091}$, and a damping of the BAO feature $\Sigma_{\rm nl} = 7.741^{+0.092}_{-0.088}$ smaller than that measured for dark matter $\Sigma_{\rm nl} = 8.231^{+0.025}_{-0.027}$. See Section 4 for a comparison with previous works found in the literature both for dark matter and haloes. The bottom panels show the likelihood χ^2 distributions for the BAO shift α parameter both for dark matter and the halo sample.

In the next section, we provide the main results of our analysis for the non-linear evolution with redshift of the shift and damping of the BAO feature for dark matter and four halo samples with different number density, both in real- and redshift-space. We also compare our results with previous works.

Table 1. Results for the estimation of the errors in the computation of the ratio $P(k)/P_{\rm nw}(k)$ used for the fitting procedure.

	DM	HALOES			
Redshift		2×10^{-3}	1×10^{-3}	4×10^{-4}	2×10^{-4}
1	0.000 314	0.001 73	0.001 75	0.002 37	0.003 20
0.741	0.000 349	0.001 82	0.001 83	0.002 41	0.003 03
0.562	0.000 362	0.001 44	0.001 84	0.002 44	0.003 44
0.358	0.000 393	0.001 27	0.001 54	0.002 15	0.003 06
0.164	0.000 431	0.001 49	0.001 60	0.002 22	0.003 36
0	0.000 475	0.001 25	0.001 68	0.002 11	0.003 25

4 RESULTS ON BAO SYSTEMATICS

4.1 Matter

We show in Table 2 and Fig. 5 our main results on the non-linear evolution with redshift of the BAO shift $\alpha - 1[\text{per cent}]$ and damping $\Sigma_{\rm nl}$ for the dark matter tracer, in real- and redshift-space, following the methodology described in Section 3. The trend of the acoustic scale shift towards $z = 0$ is measured at high precision, which together with the good sampling in redshift, allow us to provide

Table 2. The best-fitting values for the BAO shift α and damping $\Sigma_{\rm nl}$ measured at different redshifts from fitting the real-space power spectrum $P(k)/P_{\rm nw}(k)$ ratio drawn from all BigMD dark matter particles. The damping computed from linear theory $\Sigma^{\rm th}_{\rm nl}$, given equation (3), is also given for comparison. Σ_{100} is the dispersion of the dark matter particle pair separation at BAO scales. The χ^2 per degree of freedom are also listed.

Redshift	$\alpha - 1$[per cent]	$\Sigma_{\rm nl}$ (Mpc h^{-1})	$\Sigma^{\rm th}_{\rm nl}$	Σ_{100}	$\chi^2/d.o.f.$
1.000	$0.148^{+0.011}_{-0.011}$	$5.185^{+0.015}_{-0.015}$	5.171	5.262	1.00
0.887	$0.161^{+0.012}_{-0.012}$	$5.440^{+0.015}_{-0.016}$	5.438	5.534	1.02
0.741	$0.182^{+0.013}_{-0.014}$	$5.795^{+0.016}_{-0.017}$	5.816	5.910	0.99
0.655	$0.194^{+0.014}_{-0.014}$	$6.024^{+0.017}_{-0.017}$	6.062	6.158	1.03
0.562	$0.212^{+0.014}_{-0.016}$	$6.288^{+0.018}_{-0.017}$	6.345	6.443	1.05
0.453	$0.231^{+0.017}_{-0.016}$	$6.617^{+0.019}_{-0.018}$	6.703	6.800	1.02
0.358	$0.251^{+0.018}_{-0.018}$	$6.923^{+0.020}_{-0.019}$	7.035	7.130	1.03
0.265	$0.273^{+0.021}_{-0.019}$	$7.242^{+0.021}_{-0.021}$	7.384	7.475	1.01
0.164	$0.301^{+0.023}_{-0.021}$	$7.605^{+0.023}_{-0.023}$	7.787	7.863	1.01
0.081	$0.327^{+0.025}_{-0.025}$	$7.916^{+0.024}_{-0.024}$	8.135	8.205	1.01
0.000	$0.353^{+0.027}_{-0.026}$	$8.231^{+0.025}_{-0.027}$	8.486	8.541	1.01

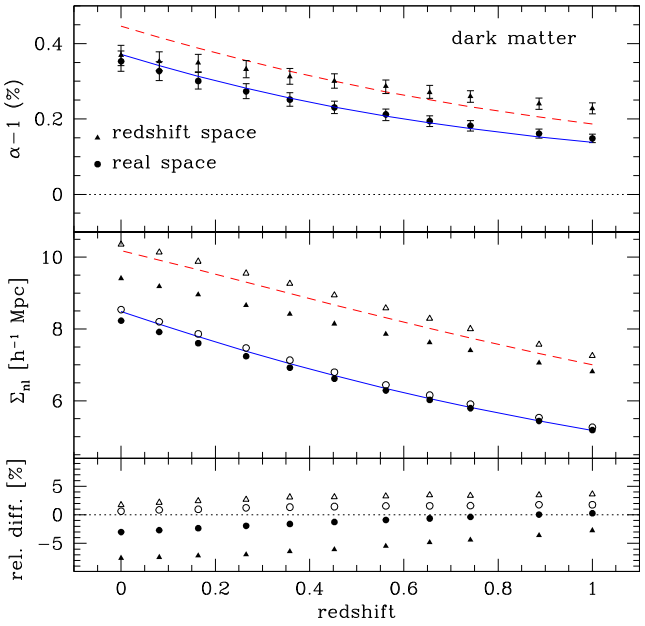

Figure 5. Non-linear evolution of the BAO shift and damping with redshift for dark matter in real- and redshift-space (solid circles and triangles, respectively). The solid line in the top and middle panel are our best fit to $\alpha(z) - 1 \propto [D(z)/D(0)]^2$ and the linear theory estimate of the damping given by equation (3), respectively. Errors for the damping measurements are smaller than the size of the symbols. The dashed lines correspond to redshift-space predictions. The open circles and triangles are representing the dispersion of the dark matter pair separation at BAO scales measured from the BigMD simulation (see the text). The bottom panel shows the relative ratio of the damping measurements as compared to linear theory.

an accurate parametrization of the evolution of α as a function of the linear growth factor $D(z)$. For the data in real-space, we find $\alpha(z) - 1[\text{per cent}] = (0.350 \pm 0.014)[D(z)/D(0)]^{1.74 \pm 0.14}$. These results are consistent with Seo et al. (2010). They based their fit of the evolution of the BAO shift $\alpha(z)$ only in three redshift measurements at $z = 0.3$, 1.0, and 3.0. Those measurements are based on a couple of boxes with volume $(2\,\text{Gpc}\,h^{-1})^3$ and 576^3 particles with force resolution of 173.6 kpc h^{-1}. For each of their individual BAO shift measurements at $z = 0.3$ and 1.0, we obtained a relative error of the BAO shift which is 3.7 and 4.5 times better, respectively. This comparison can be done by taking our data listed in Table 2, and table 2 in Seo et al. (2010). Indeed, Seo et al. (2010) reached similar accuracy than us when using the simulations of Takahashi et al. (2009). Yet, this result was reported only at $z = 0$, and was not used to constraint the evolution of α. We also note that as compared to Seo et al. (2010), we have 6.5 and 2.5 better relative error in the determination of the zero-point and power-law exponent of the $\alpha(z)$ parametrization.

The measured power index in $\alpha(z)$ is close to the expected $D(z)^2$ prediction from perturbation theory (see Padmanabhan & White 2009; Sherwin & Zaldarriaga 2012). In this case, if we fix the power index to 2, we obtained $\alpha(z) - 1[\text{per cent}] = (0.3716 \pm 0.0083)[D(z)/D(0)]^2$ (solid line in the top panel of Fig. 5).

Moreover, the evolution of the BAO damping in real-space as a function of redshift agrees remarkably well, within 0.25 per cent at $z = 1$ and 3 per cent at $z = 0$, with that from linear theory shown in the middle panel of Fig. 5 as solid line (see also bottom panel for the relative ratio), as previously reported by Sánchez et al. (2008) and Crocce & Scoccimarro (2008); where the broadening

Table 3. As in Table 2 but for redshift-space.

Redshift	$\alpha - 1$[per cent]	$\Sigma_{\rm nl}$ (Mpc h^{-1})	Σ_{100}	$\chi^2/d.o.f.$
1.000	$0.228^{+0.015}_{-0.015}$	$6.814^{+0.017}_{-0.016}$	7.257	0.98
0.887	$0.241^{+0.015}_{-0.015}$	$7.056^{+0.016}_{-0.017}$	7.572	1.04
0.741	$0.256^{+0.015}_{-0.016}$	$7.406^{+0.017}_{-0.016}$	8.010	1.14
0.655	$0.271^{+0.018}_{-0.016}$	$7.626^{+0.018}_{-0.017}$	8.291	1.06
0.562	$0.287^{+0.017}_{-0.019}$	$7.858^{+0.017}_{-0.018}$	8.584	1.06
0.453	$0.301^{+0.019}_{-0.019}$	$8.147^{+0.019}_{-0.019}$	8.942	1.02
0.358	$0.313^{+0.021}_{-0.020}$	$8.415^{+0.018}_{-0.021}$	9.268	1.06
0.265	$0.332^{+0.023}_{-0.023}$	$8.657^{+0.021}_{-0.021}$	9.553	1.02
0.164	$0.349^{+0.023}_{-0.024}$	$8.959^{+0.021}_{-0.023}$	9.881	1.08
0.081	$0.353^{+0.026}_{-0.025}$	$9.185^{+0.024}_{-0.022}$	10.135	1.02
0.000	$0.369^{+0.026}_{-0.027}$	$9.410^{+0.024}_{-0.025}$	10.358	1.01

and attenuation of the BAO feature is exponential, as adopted in our model, with a scale $\Sigma_{\rm nl}^{\rm th}$ computed following Crocce & Scoccimarro (2006) and Matsubara (2008), i.e.

$$\Sigma_{\rm nl}^{\rm th} = \left[\frac{1}{3\pi^2}\int P_{\rm lin}(k)\,{\rm d}k\right]^{1/2}. \quad (3)$$

BAO damping is basically introduced by the dispersion of pair separations at BAO scales. Similar to Eisenstein et al. (2007), in our Table 2, we also show the rms of the displacements of the dark matter particle pairs with initial separations $\sim 100\,h^{-1}$ Mpc, Σ_{100}. The displacement is defined as the difference between the initial separation and the separation at given redshift in the radial direction (along the line connecting the pair). The dispersion of the separations are consistent with our BAO damping measurements in 1–2 per cent (see also Fig. 5).

In Table 3 and Fig. 5, we also provide the shift and damping measurements in redshift-space. In agreement with e.g. Sánchez et al. (2008), Crocce & Scoccimarro (2008) and Seo et al. (2010), we measure BAO shifts in redshift-space which are larger than in real-space. An increase of the shift is expected due to RSD induced by peculiar velocities. In linear perturbation theory of gravitational instability the Lagrangian displacement in the ZA is larger along the line-of-sight direction by a factor $(1 + f)$, where $f = {\rm d}\ln D/{\rm d}\ln a \approx \Omega_{\rm m}^{0.55}(z)$ is the logarithmic derivative of the linear growth rate (Eisenstein et al. 2007). Hence, for a spherically averaged power spectrum in redshift-space we expect a shift increase of $\approx[((1 + f)^2 + 2)/3]^{1/2}$ (being $\sim 1 + f/3$ also a good approximation as adopted in Seo et al. 2010). The dashed line in the top panel of Fig. 5 shows the theoretical prediction for the shift of the acoustic scale in redshift-space adopting our best fit to $\alpha(z) - 1 \propto [D(z)/D(0)]^2$ for the shift evolution in real-space (solid line). The simulation and model shift results agree well within $\sim$20 per cent over the entire redshift range. Following the same argument in linear theory, there should be also an increase of the BAO damping in redshift-space by the same f-factor as compared to that in real-space. Indeed, this is what we find as shown in the middle panel of Fig. 5. The dashed line shows the redshift-space linear prediction for the BAO damping after we adopt equation (3) for the real-space theory estimate. The agreement with our simulation results is better than $\sim$10 per cent over the entire redshift range (see bottom panel of Fig. 5), with an increasing departure towards $z = 0$ due to non-linear effects. In Table 3 and Fig. 5, we also show the rms of the displacements of the dark matter particle pairs with initial separations $\sim 100\,h^{-1}$ Mpc in redshift space. The agreement

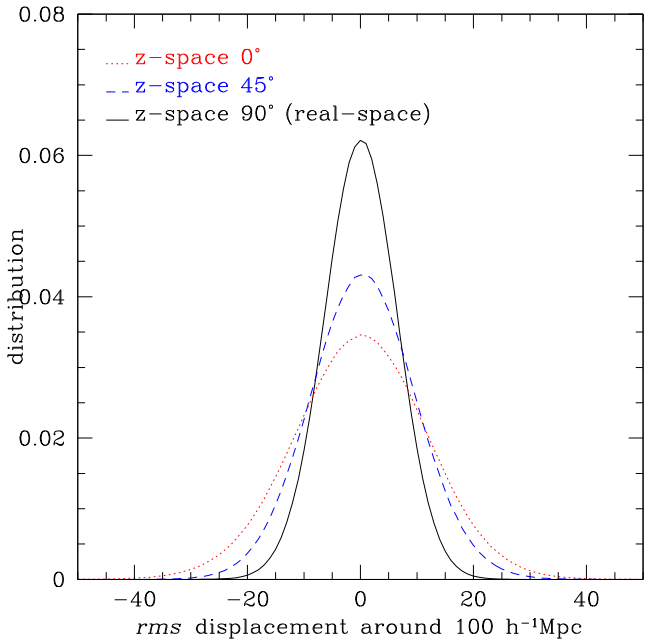

Figure 6. The rms of the displacements with initial separation of $\sim 100\,h^{-1}$ Mpc in redshift-space. We select the pairs in three different directions, 0°, 45°, and 90° with respect to the line of sight, of which the one in 90° (in the transverse direction) is the same as the displacement in real-space since we only are interested in the radial direction (along the line connecting the pairs). One can see that the dispersion is larger when the angle between the pair and line of sight is smaller. The dispersion of the separations will erase the clustering signal and result in BAO damping.

is not as good as in real-space. It might indicate that the spherically averaged BAO damping cannot be derived perfectly from the spherically averaged rms of the displacement because of anisotropy. This is shown in Fig. 6 where we plot the rms of the displacements with initial separation of $\sim 100\,h^{-1}$ Mpc in redshift space. We select the pairs in three different directions, 0°, 45°, and 90° with respect to the line of sight, of which the one in 90° – in the transverse direction – is the same as the displacement in real-space since we only are interested in the radial direction (along the line connecting the pairs). One can see that the dispersion is larger when the angle between the pair and line of sight is smaller. The dispersion of the separations will erase the clustering signal and result in BAO damping.

4.2 Haloes

We provide in Table 4 the best-fitting values of the BAO shift and damping measured at different redshifts up to $z = 1$ for four BigMD dark matter halo samples, in real-space, with number densities 2×10^{-3}, 1×10^{-3}, 4×10^{-4}, $2 \times 10^{-4}\,h^3\,\mathrm{Mpc}^{-3}$; which scan a halo bias range from 1.2 to 2.8 over the entire explored redshift range. We measure in all halo samples a typical BAO shift of ≈0.25 per cent which does not seems to evolve with redshift within the errors, that range from ∼0.065 per cent for the denser halo sample with number density $2 \times 10^{-3}\,h^3\,\mathrm{Mpc}^{-3}$ to ∼0.14 per cent in the case of the sparsest sample with $n = 2 \times 10^{-4}\,h^3\,\mathrm{Mpc}^{-3}$. We summarize our BAO shift results for the halo tracers in Fig. 7. We plot the shift $\alpha - 1$[per cent] as a function of halo bias at $z = 0$, where we have adopted the assumption that $b(z = 0) \equiv b(z)D(z = 0)/D(z)$ (Lahav et al. 2002). For each halo sample, we plot with different tiny solid symbols for the different redshifts (colour coded) each of the individual BAO shift measurements. Additionally, large open circles shows the mean values of the shift measurements for the four bias bins, and 1σ error bars correspond to the errors of the mean. We obtain $\alpha - 1$[per cent] shifts 0.216 ± 0.065, 0.216 ± 0.076, 0.275 ± 0.099 and 0.267 ± 0.140 for a mean halo bias of 1.17, 1.32, 1.53, and 1.71, respectively. The size of the bias bins are about the diameter of the open symbols. Thus, we conclude there is a flat dependence of the BAO shift as a function of halo bias in our BigMD Planck simulations. We note the higher accuracy reached by our study of the shift in the acoustic scale for halo tracers as compared with previous works found in the literature. For different HOD samples, Mehta et al. (2011) reported larger errors, and did not detect any shift in the BAO, but found some moderate shifts for their most biased models. We also contradict the negative BAO shifts found by Sánchez et al. (2008) in their FoF halo samples. On the other hand, we agree qualitatively with the recent work of Angulo et al. (2014), although a fair comparison is hard because they measured the BAO shift for galaxy samples built from their semi-analytical models of galaxy formation, and only reported results at $z = 1$.

Our results has to be reconciled with perturbation theory predictions found in the literature that predicted an increase of the shift with halo bias (Padmanabhan & White 2009). A better understanding of the non-local bias would be required to allow the proper shifts of the acoustic scale reported in this work for the halo tracers. Understanding this BAO systematics is key, and represent a serious challenge for future redshift surveys, such as DESI and *Euclid*, that aim to reach an accuracy in the BAO scale better than ∼0.3 per cent. Redshift-space estimates for the BAO shifts are provided in Table 5. Results, in general, may suggest a larger shift as compared to real-space as previously reported (e.g. Sánchez et al. 2008), although they are not as convincing given their larger errors, about ∼1.5–2 times larger than real-space uncertainties (see Table 4).

Our measurement results in real-space on the evolution with redshift of the BAO damping for our four BigMD halo samples are also given in Table 4. We report a different behaviour as that seen, and discussed above, for the dark matter tracer. This is clearly observed in Fig. 8, where we see that the damping $\Sigma_{\rm nl}$ measurements in haloes decreases down to ∼10–15 per cent with decreasing redshift as compared to dark matter, represented in the plot by a solid line that connects the measurements listed in Table 2, and shown in Fig. 5 as open triangles. We also notice, at a given redshift, less damping of the BAO signature for halo samples with smaller number densities, i.e. larger halo bias (see bottom panel of Fig. 8). In summary, from our analysis we can conclude that the acoustic feature for haloes suffers less broadening due to non-linear effects than for dark matter, and remarkably, damping of the acoustic oscillations in haloes seems to depends mildly on bias. This result was already suggested by Wang & Zhan (2013, see also Angulo et al. 2014), although they did not report a quantitative measurement of the BAO damping as a function of redshift as that presented in our Fig. 5.

The smaller damping seen in the BAO signal for halo tracers is highlighted in Fig. 9 when we show the ratio of the scale-dependent halo bias in the BigMDPL simulation with acoustic oscillations to that in the non-wiggle BigMDPLnw simulation for the measurements of the $z = 0$ halo sample with number density $1 \times 10^{-3}\,\mathrm{Mpc}^{-3}\,h^3$ (bias = 1.33) shown in Fig. 3, i.e. $b(k)/b_{\rm nw}(k) \equiv [P^h(k)/P^{\rm dm}(k)]/[P^{\rm h}_{\rm nw}(k)/P^{\rm dm}_{\rm nw}(k)]$ (solid circles). The solid line represents the best-fitting model to the data as discussed in Section 3. A clear modulation in phase with the acoustic scale is observed in the halo bias, with an amplitude of ∼0.25 per cent, due to the

Table 4. The best-fitting values for the BAO shift α and damping $\Sigma_{\rm nl}$ measured at several redshifts from fitting the $P(k)/P_{\rm nw}(k)$ ratio, in real-space, drawn from four different number densities (and bias) BigMD halo samples. The χ^2 per degree of freedom are also provided.

$n = 2.0 \times 10^{-3}$	$z = 0$	0.164	0.358	0.562	0.741	1.000
Bias	1.19	1.29	1.42	1.56	1.70	1.91
$\alpha - 1$[per cent]	$0.241^{+0.066}_{-0.067}$	$0.165^{+0.074}_{-0.074}$	$0.123^{+0.060}_{-0.052}$	$0.087^{+0.060}_{-0.063}$	$0.318^{+0.070}_{-0.069}$	$0.356^{+0.062}_{-0.063}$
$\Sigma_{\rm nl}$	$7.757^{+0.065}_{-0.068}$	$7.048^{+0.078}_{-0.075}$	$6.513^{+0.063}_{-0.061}$	$6.284^{+0.068}_{-0.072}$	$5.732^{+0.078}_{-0.079}$	$5.335^{+0.074}_{-0.074}$
χ^2/dof	1.32	1.11	1.40	1.13	1.38	1.48
$n = 1.0 \times 10^{-3}$						
Bias	1.33	1.44	1.59	1.76	1.92	2.16
$\alpha - 1$[per cent]	$0.236^{+0.086}_{-0.091}$	$0.083^{+0.074}_{-0.086}$	$0.162^{+0.066}_{-0.070}$	$0.217^{+0.076}_{-0.081}$	$0.266^{+0.076}_{-0.073}$	$0.333^{+0.065}_{-0.065}$
$\Sigma_{\rm nl}$	$7.741^{+0.092}_{-0.087}$	$6.834^{+0.082}_{-0.078}$	$6.427^{+0.075}_{-0.075}$	$6.289^{+0.090}_{-0.087}$	$5.994^{+0.090}_{-0.085}$	$5.340^{+0.084}_{-0.080}$
χ^2/dof	0.99	1.25	1.22	0.99	1.03	1.30
$n = 4.0 \times 10^{-4}$						
Bias	1.54	1.67	1.84	2.04	2.22	2.50
$\alpha - 1$[per cent]	$0.379^{+0.106}_{-0.103}$	$0.133^{+0.099}_{-0.114}$	$0.231^{+0.098}_{-0.094}$	$0.377^{+0.098}_{-0.095}$	$0.277^{+0.103}_{-0.089}$	$0.25^{+0.096}_{-0.085}$
$\Sigma_{\rm nl}$	$7.430^{+0.120}_{-0.103}$	$6.728^{+0.106}_{-0.110}$	$6.408^{+0.108}_{-0.098}$	$6.081^{+0.120}_{-0.115}$	$5.542^{+0.124}_{-0.108}$	$5.182^{+0.114}_{-0.107}$
χ^2/dof	1.25	1.18	1.28	1.02	0.97	1.12
$n = 2.0 \times 10^{-4}$						
Bias	1.73	1.88	2.07	2.28	2.49	2.80
$\alpha - 1$[per cent]	$0.451^{+0.162}_{-0.170}$	$0.127^{+0.150}_{-0.165}$	$0.434^{+0.129}_{-0.147}$	$0.265^{+0.135}_{-0.131}$	$0.350^{+0.118}_{-0.122}$	$0.111^{+0.122}_{-0.117}$
$\Sigma_{\rm nl}$	$7.550^{+0.171}_{-0.171}$	$6.557^{+0.168}_{-0.157}$	$6.015^{+0.136}_{-0.136}$	$5.931^{+0.162}_{-0.171}$	$5.159^{+0.144}_{-0.130}$	$4.928^{+0.137}_{-0.147}$
χ^2/dof	0.83	0.88	1.02	0.88	1.09	1.03

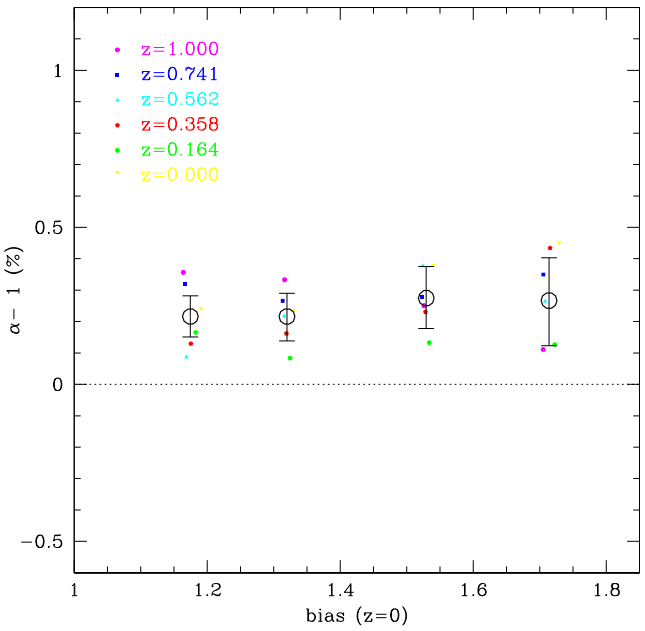

Figure 7. Measurements of the BAO shift as a function of halo bias for our BigMD Planck data. Each of the individual shift estimates are shown with tiny solid symbols for the different redshifts (colour coded). Large open circles show the mean values for the four bias bins, and 1σ error bars correspond to the errors of the mean.

presence of the BAOs. It is worth mentioning the work by Wang & Zhan (2013), who using much worse numerical resolution and significantly less volume in their simulations, but performing many realizations and taking advantage of using non-wiggle realizations, did also detect this signature in the halo bias due to the BAO for a halo sample with two order of magnitude $\sim 10^{-3}$ Mpc^{-3} h^3 higher number density, where they detected a modulation amplitude of $\sim$0.5 per cent due to the much larger bias of their sample ($b > 3$, see bottom panel of their fig. 4).

For all halo samples and redshifts, we clearly observe a larger BAO damping in redshift-space. Our measurements are provided in Table 5, and within the errors they can be explained well by adopting a shift increase of $\approx[((1+f)^2+2)/3]^{1/2}$ due to RSD, as discussed above.

5 SUMMARY

We study, from redshift 1 to the present, the non-linear evolution of the shift and damping of BAOs in the power spectrum of dark matter and halo tracers using cosmological simulations with high-mass resolution over a large volume. The results presented in this paper are based on the BigMD suite of simulations in the standard ΛCDM cosmology, with numerical parameters (mass and force resolution) that have been chosen to face the requirements imposed by current and future dark energy experiments on understanding any possible systematic shifts in the BAO signal due to non-linear gravitational growth, scale-dependent bias and RSD to a high precision, better than the measured statistical uncertainties. Our measurements can also be useful for comparison with perturbation theory works that aim at explaining the nature of BAO shift and damping in dark matter and haloes. We compare our results with previous works.

Our main results can be summarized as follows.

(i) For a given tracer, we measure at several redshifts the BAO shift α and damping $\Sigma_{\rm nl}$ by fitting the ratio $P/P_{\rm nw}$ of the power spectrum with acoustic oscillations to that with non-wiggle drawn from the Planck BigMDPL/BigMDPLnw simulation pair, adopting the model given in equation (2). The effect of cosmic variance is largely reduced when dividing by the no-BAO power spectrum, which together with the proper numerical resolution and large

Table 5. Same as Table 4 but for redshift-space.

$n = 2.0 \times 10^{-3}$	$z = 0$	0.164	0.358	0.562	0.741	1.000
$\alpha - 1$[per cent]	$0.264^{+0.124}_{-0.113}$	$0.224^{+0.093}_{-0.097}$	$0.212^{+0.087}_{-0.097}$	$0.140^{+0.079}_{-0.089}$	$0.403^{+0.074}_{-0.071}$	$0.435^{+0.063}_{-0.063}$
$\Sigma_{\rm nl}$	$9.270^{+0.105}_{-0.097}$	$8.733^{+0.088}_{-0.086}$	$8.092^{+0.081}_{-0.084}$	$7.935^{+0.078}_{-0.080}$	$7.522^{+0.071}_{-0.075}$	$7.093^{+0.064}_{-0.067}$
χ^2/dof	0.92	1.09	1.32	1.04	1.15	1.53
$n = 1.0 \times 10^{-3}$						
$\alpha - 1$[per cent]	$0.358^{+0.134}_{-0.136}$	$0.167^{+0.126}_{-0.133}$	$0.281^{+0.120}_{-0.111}$	$0.287^{+0.110}_{-0.116}$	$0.391^{+0.095}_{-0.098}$	$0.473^{+0.093}_{-0.083}$
$\Sigma_{\rm nl}$	$9.312^{+0.129}_{-0.115}$	$8.547^{+0.126}_{-0.120}$	$8.108^{+0.107}_{-0.107}$	$7.932^{+0.108}_{-0.109}$	$7.720^{+0.099}_{-0.093}$	$7.064^{+0.093}_{-0.090}$
χ^2/dof	0.82	0.99	0.86	0.84	0.83	1.08
$n = 4.0 \times 10^{-4}$						
$\alpha - 1$[per cent]	$0.409^{+0.174}_{-0.157}$	$0.217^{+0.165}_{-0.173}$	$0.258^{+0.170}_{-0.170}$	$0.399^{+0.166}_{-0.162}$	$0.323^{+0.126}_{-0.125}$	$0.448^{+0.118}_{-0.117}$
$\Sigma_{\rm nl}$	$9.101^{+0.149}_{-0.147}$	$8.325^{+0.147}_{-0.146}$	$8.066^{+0.156}_{-0.157}$	$7.766^{+0.163}_{-0.171}$	$7.310^{+0.131}_{-0.125}$	$7.030^{+0.128}_{-0.122}$
χ^2/dof	0.91	1.06	0.874	0.67	0.91	0.90
$n = 2.0 \times 10^{-4}$						
$\alpha - 1$[per cent]	$0.630^{+0.304}_{-0.309}$	$0.127^{+0.255}_{-0.260}$	$0.434^{+0.264}_{-0.242}$	$0.402^{+0.235}_{-0.233}$	$0.358^{+0.198}_{-0.208}$	$0.185^{+0.165}_{-0.171}$
$\Sigma_{\rm nl}$	$9.403^{+0.275}_{-0.256}$	$8.094^{+0.234}_{-0.246}$	$7.753^{+0.213}_{-0.226}$	$7.591^{+0.243}_{-0.244}$	$6.983^{+0.205}_{-0.199}$	$6.782^{+0.179}_{-0.185}$
χ^2/dof	0.63	0.80	0.82	0.60	0.72	0.79

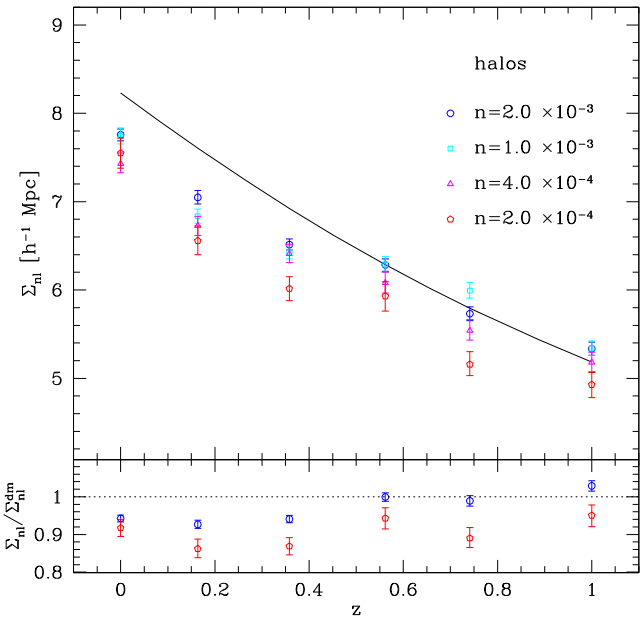

Figure 8. Non-linear evolution of the BAO damping with redshift, in real-space, for our four different halo samples (open symbols). The solid line connects the measurements for the dark matter tracer provided in Table 2 and shown in Fig. 5. The acoustic feature suffers less damping due to non-linear effects as compare to dark matter towards lower redshift and also for more sparse halo samples at a given redshift.

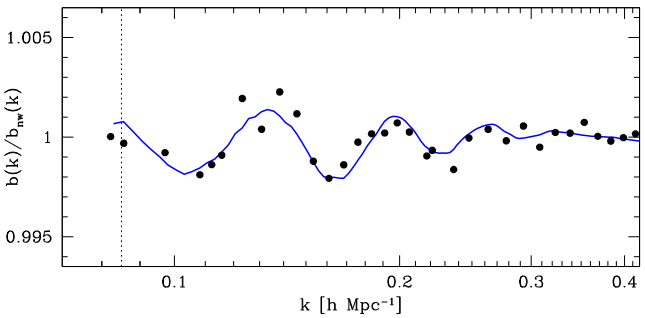

Figure 9. Ratio of the halo bias at $z = 0$ in the BigMD Planck simulation to that in the non-wiggle realization for the halo sample with $n = 1 \times 10^{-3}$ Mpc^{-3} h^3 and bias 1.33(solid symbols). Our best-fitting model is also shown with a solid line.

volume allow us to report measurements of the BAO shift and damping with high accuracy.

(ii) For dark matter, we report shifts of the acoustic scale towards larger k, relative to the linear power spectrum, measured with higher precision than previously reported in the literature. This, together with the good sampling in redshift allow us to provide an accurate parametrization of the evolution of α as a function of the linear growth factor $D(z)$, i.e. $\alpha(z) - 1[\text{per cent}] = (0.350 \pm 0.014)[D(z)/D(0)]^{1.74 \pm 0.14}$ for the data in real-space. And we find $\alpha(z) - 1[\text{per cent}] = (0.3716 \pm 0.0083)[D(z)/D(0)]^2$ if we fix the power index to 2, as expected from perturbation theory. Furthermore, the evolution of BAO damping $\Sigma_{\rm nl}$ in real-space agrees remarkably well with that from linear theory as given by equation (3). In redshift-space, we measure an increase of the shift and damping as compared to real-space, as previously reported, which is well described in linear theory by a constant factor that depends on f, the logarithmic derivative of the linear growth rate.

(iii) We measure BAO shift and damping also for four halo samples with number densities that scan a halo bias ranging from 1.2 to 2.8 over the entire explored redshift range. Our BigMD simulations allow us to resolve well haloes and subhaloes in those samples. We measure in all halo samples a typical BAO shift of ≈0.25 per cent in real-space, which does not seem to evolve with redshift within the uncertainties. Moreover, we report a constant shift as a function of halo bias. These new results clarify the previously reported works found in the literature. Redshift-space measurements are also performed, although the larger errors prevent us from a conclusive larger shift as compared to real-space. The damping of the acoustic feature for all halo samples shows a different behaviour as compared to that for dark matter. In summary, we see that haloes suffer less damping, with some weak dependence on bias. A larger BAO

damping is measured in redshift-space, which can be well explained by an increase of an f-dependent factor in linear theory due to RSD.

(iv) A clear modulation in phase with the acoustic scale is observed in the scale-dependent halo bias due to the presence of the BAOs when we study the ratio of the scale-dependent bias in the BigMD simulation with BAO to that in the 'BAO-free' simulation. This result motivates a better understanding of non-local bias.

ACKNOWLEDGEMENTS

We would like to thank Martin Crocce, Daniel Eisenstein, Nikhil Padmanabhan, Uros Seljak, and Hee-Jong Seo for useful discussions. CC and FP acknowledge support from the Spanish MICINNs Consolider-Ingenio 2010 Programme under grant MultiDark CSD2009-00064, AYA2010-21231-C02-01, MINECO Centro de Excelencia Severo Ochoa Programme under grant SEV-2012-0249, and grant AYA2014-60641-C2-1-P. CGS acknowledges funding from the Spanish MINECO under the project AYA2012-3972-C02-01. GY thanks support from the Spanish MINECO under research grants AYA2012-31101 and FPA2012-34694. CZ acknowledges support from Charling Tao and her grant from Tsinghua University, and 973 programme no. 2013CB834906. CZ also thanks the support from the MultiDark summer student programme to visit the Instituto de Física Teórica UAM/CSIC. The BigMD simulations have been performed on the SuperMUC supercomputer at the Leibniz-Rechenzentrum (LRZ) in Munich, using the computing resources awarded to the PRACE project number 2012060963.

REFERENCES

Alimi J.-M. et al., 2012, preprint (arXiv:1206.2838)
Anderson L. et al., 2014, MNRAS, 441, 24
Angulo R. E., Baugh C. M., Frenk C. S., Lacey C. G., 2008, MNRAS, 383, 755
Angulo R. E., Springel V., White S. D. M., Jenkins A., Baugh C. M., Frenk C. S., 2012, MNRAS, 426, 2046
Angulo R. E., White S. D. M., Springel V., Henriques B., 2014, MNRAS, 442, 2131
Blake C. et al., 2011, MNRAS, 415, 2892
Chuang C.-H., Wang Y., Hemantha M. D. P., 2012 MNRAS, 423, 1474
Cole S. et al., 2005, MNRAS, 362, 505
Conroy C., Wechsler R. H., Kravtsov A. V., 2006, ApJ, 647, 201
Crocce M., Scoccimarro R., 2006 Phys. Rev. D, 73, 063520
Crocce M., Scoccimarro R., 2008, Phys. Rev. D, 77, 023533
Crocce M., Fosalba P., Castander F. J., Gaztañaga E., 2010, MNRAS, 403, 1353
Eisenstein D. J. et al., 2005, ApJ, 633, 560
Eisenstein D. J., Seo H.-J., White M. J., 2007, ApJ, 664, 660
Kim J., Park C., Rossi G., Lee S. M., Gott J. R., III, 2011, J. Korean Astron. Soc., 44, 217
Kitaura F.-S., Heß S., 2013, MNRAS, 435, L78
Kitaura F.-S., Gil-Marín H., Scóccola C., Chuang C.-H., Müller V., Yepes G., Prada F., 2015, MNRAS, 450, 1836
Kitaura F.-S., Yepes G., Prada F., 2014, MNRAS, 439, L21
Kitaura F.-S., Gil-Marín H., Scóccola C. G., Chuang C.-H., Müller V., Yepes G., Prada F., 2015, MNRAS, 450, 1836
Klypin A., Holtzman J., 1997, preprint (astro-ph/9712217)
Klypin A., Prada F., Yepes G., Heß S., Gottlöber S., 2015, MNRAS, 447, 3693
Klypin A., Yepes G., Gottlober S., Prada F., Hess S., 2014, preprint (arXiv:1411.4001)
Lahav O. et al., 2002, MNRAS, 333, 961
Laureijs R. et al., 2011, preprint (arXiv:1110.3193)
Lawrence E., Heitmann K., White M., Higdon D., Wagner C., Habib S., Williams B., 2010, ApJ, 713, 1322
Levi M. et al., 2013, preprint (arXiv:1308.0847)
Lewis A., Challinor A., Lasenby A., 2000 ApJ, 538, 473
Matsubara T., 2008, Phys. Rev. D, 77, 063530
McBride C., Berlind A., Scoccimarro R., Wechsler R., Busha M., Gardner J., van den Bosch F., 2009, BAAS, 41, 425.06
Mehta K. T., Seo H.-J., Eckel J., Eisenstein D. J., Metchnik M., Pinto P., Xu X., 2011, ApJ, 734, 94
Neyrinck M. C., Yang L. F., 2013, MNRAS, 433, 1628
Nuza S. E. et al., 2013, MNRAS, 432, 743
Padmanabhan N., White M., 2009, Phys. Rev. D, 80, 063508
Padmanabhan N., Xu X., Eisenstein D. J., Scalzo R., Cuesta A. J., Mehta K. T., Kazin E., 2012, MNRAS, 427, 2132
Percival W. J., Cole S., Eisenstein D. J., Nichol R. C., Peacock J. A., Pope A. C., Szalay A. S., 2007, MNRAS, 381, 1053
Planck Collaboration XVI, 2014, A&A, 571, A16
Prada F., Klypin A. A., Cuesta A. J., Betancort-Rijo J. E., Primack J., 2012, MNRAS, 423, 3018
Press W. H., Teukolsky S, A. Vetterling W. T., Flannery B. P., 1992, Numerical Recipes in FORTRAN, The Art of Scientific Computing. Cambridge Univ. Press, Cambridge
Rasera Y., Corasaniti P.-S., Alimi J.-M., Bouillot V., Reverdy V., Balmès I., 2014, MNRAS, 440, 1420
Reid B. A. et al., 2010, MNRAS, 404, 60
Riebe K. et al., 2013, Astron. Nachr., 334, 691
Sánchez A. G., Baugh C. M., Angulo R. E., 2008, MNRAS, 390, 1470
Sanchez A. G., Crocce M., Cabre A., Baugh C. M., Gaztanaga E., 2009, MNRAS, 400, 1643
Schlegel D. et al., 2011, preprint (arXiv:1106.1706)
Schneider A. et al., 2015, preprint (arXiv:1503.05920)
Seo H.-J., Siegel E. R., Eisenstein D. J., White M., 2008, ApJ, 686, 13
Seo H.-J. et al., 2010, ApJ, 720, 1650
Sherwin B. D., Zaldarriaga M., 2012, Phys. Rev. D, 85, 103523
Skillman S. W., Warren M. S., Turk M. J., Wechsler R. H., Holz D. E., Sutter P. M., 2014, preprint (arXiv:1407.2600)
Smith R. E., Scoccimarro R., Sheth R. K., 2008, Phys. Rev. D, 77, 043525
Smith R. E., Reed D. S., Potter D., Marian L., Crocce M., Moore B., 2014, MNRAS, 440, 249
Takahashi R. et al., 2009, ApJ, 700, 479
Teyssier R. et al., 2009, A&A, 497, 335
Trujillo-Gomez S., Klypin A., Primack J., Romanowsky A. J., 2011, ApJ, 742, 16
Wang Q., Zhan H., 2013, ApJ, 768, L27
Watson W. A., Iliev I. T., D'Aloisio A., Knebe A., Shapiro P. R., Yepes G., 2013, MNRAS, 433, 1230
Weinberg D. H., Mortonson M. J., Eisenstein D. J., Hirata C., Riess A. G., Rozo E., 2013, Phys. Rep., 530, 87

This paper has been typeset from a TEX/LATEX file prepared by the author.